ELSEVIER

Chemical Engineering Journal 87 (2002) 329–338

Chemical Engineering Journal

www.elsevier.com/locate/cej

Drying kinetics of single porous particles in superheated steam under pressure

Art Yew Looi, Kurt Golonka, Martin Rhodes*

Department of Chemical Engineering, Monash University, P.O. Box 36, Melbourne 3800, Vic., Australia

Received 23 April 2001; received in revised form 10 October 2001; accepted 15 October 2001

Abstract

The kinetics of single porous particles of ceramic and lignite in pressurised superheated steam was investigated experimentally. Particles of diameters in the range 10–14 mm were used. The experiments were performed over a range of pressure, from 1.7 to 8.4 bar, and a range of superheated steam temperature, from 155 to 197 °C. The steam velocity was also varied, from 1.1 to 4.3 m/s. The results from these experiments show that the rate of drying is limited by the rate of external convective heat transfer. The operating pressure appears to have no influence on the drying rate. The experimental results, however, show that the equilibrium moisture content is higher in a higher pressure steam and that this equilibrium is attained earlier when drying is carried at higher pressure. A mathematical model for the drying of single particles in pressurised superheated steam was also developed and tested against experimental results of ceramic drying. This model is based on the receding core assumption and is solved using the Crank–Nicholson method. Prediction of drying rate, drying time and moisture content in the case of porous ceramic particles is encouraging. In the case of lignite particles the model always under-predicts the drying rate and this is thought to be due to cracking of the lignite particles which increases the area for heat transfer.

Keywords: Steam drying; Single particle; Pressure; Lignite

1. Introduction

According to the publication of Hausbrand [1], the concept of drying in superheated steam was first discussed in 1908 but significant industrial application was not documented until 1920 [2].

Drying in superheated steam offers significant advantages over air drying; it has a higher thermal efficiency, it offers the possibility of recovery of the latent heat of evaporation, and gas volumes handled are much lower.

The study reported here is part of a larger project to investigate the possibility of drying Victorian lignite, which has a typical raw moisture content of 60%, in pressurised superheated steam in a fluidized bed, prior to combustion or gasification.

In this paper, we present the characterisation, by experiment and numerical modelling, of the drying kinetics of single porous particles in a pressurised superheated steam environment. The materials used are lignite (the subject of the broader investigation) and ceramic, which is used as an ideal, uniform porous particle. The numerical model is tested against the experimental results of drying particles of both ceramic and lignite.

2. Experimental

A bench scale apparatus was designed and fabricated for the purpose of this work. It was designed such that the rate of mass loss and the internal temperature of a particle could be continuously and simultaneously measured when drying was carried out in a pressurised superheated steam environment.

The drying chamber, as shown schematically in Fig. 1, was assembled using standard pipe fittings. The inside diameter and the length of the drying chamber were approximately 25 and 100 mm, respectively. The chamber was insulated with 50 mm thick mineral wool.

Two similar particles of predetermined size were located in the drying chamber during each experiment. One of them had a thermocouple inserted with its junction positioned at the centre of the particle. The second particle was placed in a wire basket which was suspended from a force transducer. It was necessary to prepare the coal particles immediately before each experiment. This was done so that the coal moisture content could be maintained as close as possible to the natural level before the commencement of each experiment.

* Corresponding author. Tel.: +61-3-9905-3445; fax: +61-3-9905-5686.
E-mail address: martin.rhodes@eng.monash.edu.au (M. Rhodes).

1385-8947/02/$ – see front matter
PII: S1385-8947(01)00244-3

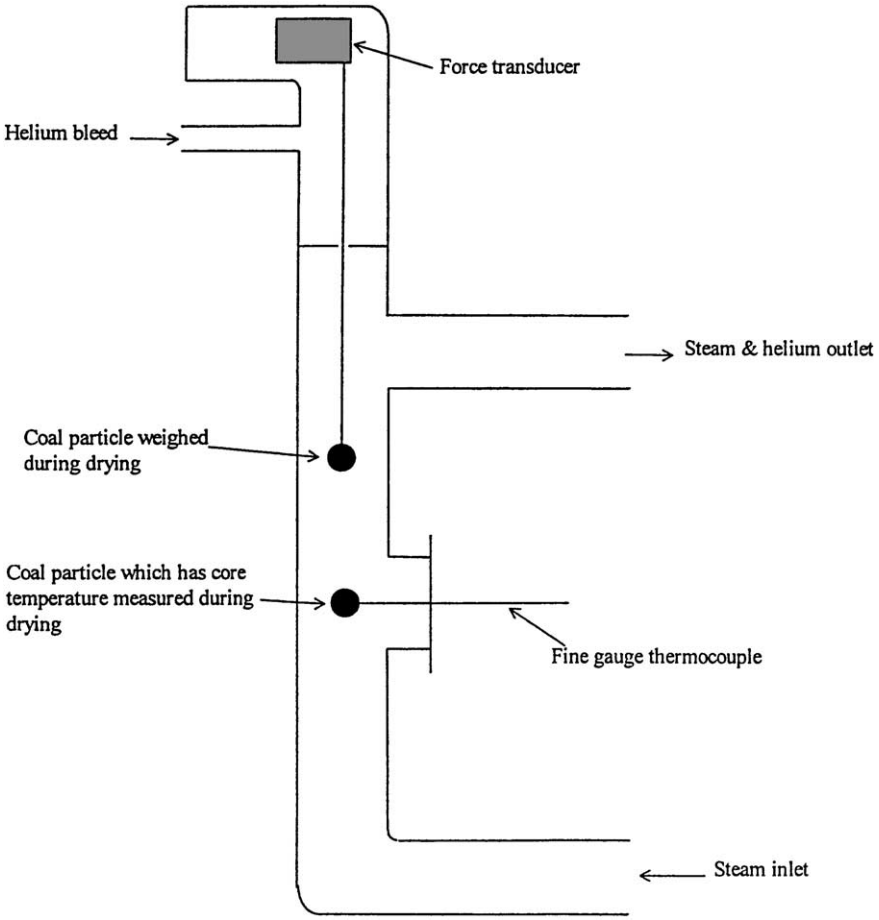

Fig. 1. Schematic diagram of the drying chamber.

The steam inlet was located at the lower end of the chamber and the steam exit at the other end. A water-cooled compartment was attached above the steam exit level. This compartment housed the load cell from which one of the two particles in the drying chamber was suspended. The section between the drying chamber and the load cell housing was also cooling water-jacketed.

The force transducer was designed to operate in an environment of lower than 80 °C temperature. It was therefore necessary to protect the transducer by means of helium gas blanketing. Helium gas of less than 5 vol.% of the total steam flow was continuously bled into the housing of the transducer and left the system with the exit steam. The vast density difference between helium and steam made it extremely unlikely that helium had any contact with the particles in the drying chamber. The exhaust gas was then driven through a condenser.

2.1. Instrumentation

The drying rate was determined by means of continuous measurement of the mass of the particle using an industrial load cell. The cell capacity was rated at 2 g force with a combined accuracy of better than ±0.5%. The temperature of the core of the coal particle was measured using a T-type thermocouple. This type of thermocouple provides an accuracy of ±0.75% of the measurement. The electrical output of these two measurements was continuously logged by a data acquisition unit.

The steam pressure in the drying chamber and the feed flowrate were regulated and controlled upstream of the drying chamber. Prior to being fed into the drying chamber, the steam was electrically heated to the required degree of superheat.

The pressure in the drying chamber was measured with a locally mounted pressure gauge at the exit of the chamber. The steam feed flowrate was measured using rotameters calibrated to deliver an accuracy of better than ±1% of measured value.

The power input to the feed superheater was controlled based on the setpoint for the feed temperature. The superheated steam temperature was measured with a K-type thermocouple, at the entry to the drying chamber. The measurements obtained were accurate to ±0.75%.

Table 1
Particle sizes and operating parameters for single particle steam drying experiments

Experiment	Material	d_p (mm)	P (bar)	T_a (°C)	v (m/s)
01	Coal	14	1.7	186	2.9
02	Coal	13	2.0	175	2.7
03	Coal	12	5.8	195	1.5
04	Coal	12	2.0	173	2.7
05	Coal	12	8.4	197	1.4
06	Coal	12	2.3	161	2.7
07	Coal	10	2.4	170	2.7
08	Coal	12	2.3	171	3.5
09	Coal	12	2.5	156	2.8
10	Coal	12	2.3	170	2.7
11	Coal	12	2.5	170	2.7
12	Coal	12	2.5	155	2.8
13	Ceramic	10	2.9	161	2.7

2.2. Experimental procedure

The cooling of the load cell housing was first initiated while the helium bleed was allowed to flood the load cell compartment. The entire steam flow path was then preheated and the previously trapped condensate was expelled from the piping. The superheater and the heating element on the drying chamber wall were also activated during the preheating period. The temperature set point was adjusted to attain the required temperature of the steam feed to the drying chamber for that particular experimental run.

Upon confirmation that the target feed steam temperature was achieved, the steam flow was diverted to by-pass the drying chamber, the heat tracer around the drying chamber wall switched off and the helium bleed stopped while the solid particles were loaded into the drying chamber appropriately.

The experiment proper commenced when steam of steady feed pressure and temperature was rediverted to the drying chamber. The flowrate of steam was controlled such that these particles did not oscillate during the experiments since oscillation was found to give rise to noisy measurements. During the experiment, particle mass and temperature were logged at 30 s intervals. The experiment ended when there was no further change in the mass of the monitored particle. Experiments were conducted at the conditions shown in Table 1.

3. Results and discussion

All the instantaneous moisture content and core temperature measurements for each experiment are presented in graphical form as in Figs. 2–7. Note that the temperature measured during Experiment 09 was that of the particle surface. In each of these figures, the preheating period is not shown. The instantaneous moisture content within each particle is represented by a dimensionless mass unit (g moisture/g dry solid).

3.1. General observation and result reproducibility

The moisture content of raw coal changes in response to the surrounding conditions [4]. In addition, the physical properties (pore size and distribution) of the coal

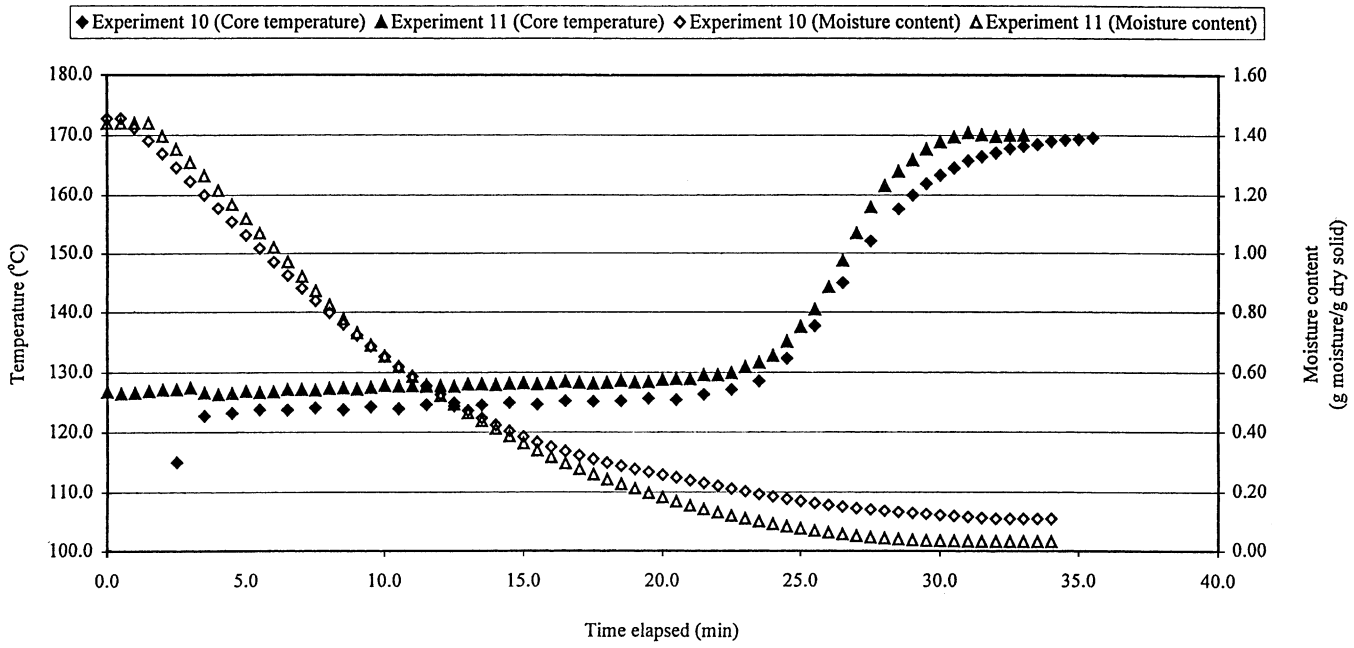

Fig. 2. Results from similar single coal particle drying experiments—Experiment 10: 12 mm, 2.7 m/s steam at 2.3 bar, 170 °C; Experiment 11: 12 mm, 2.7 m/s steam at 2.5 bar, 170 °C.

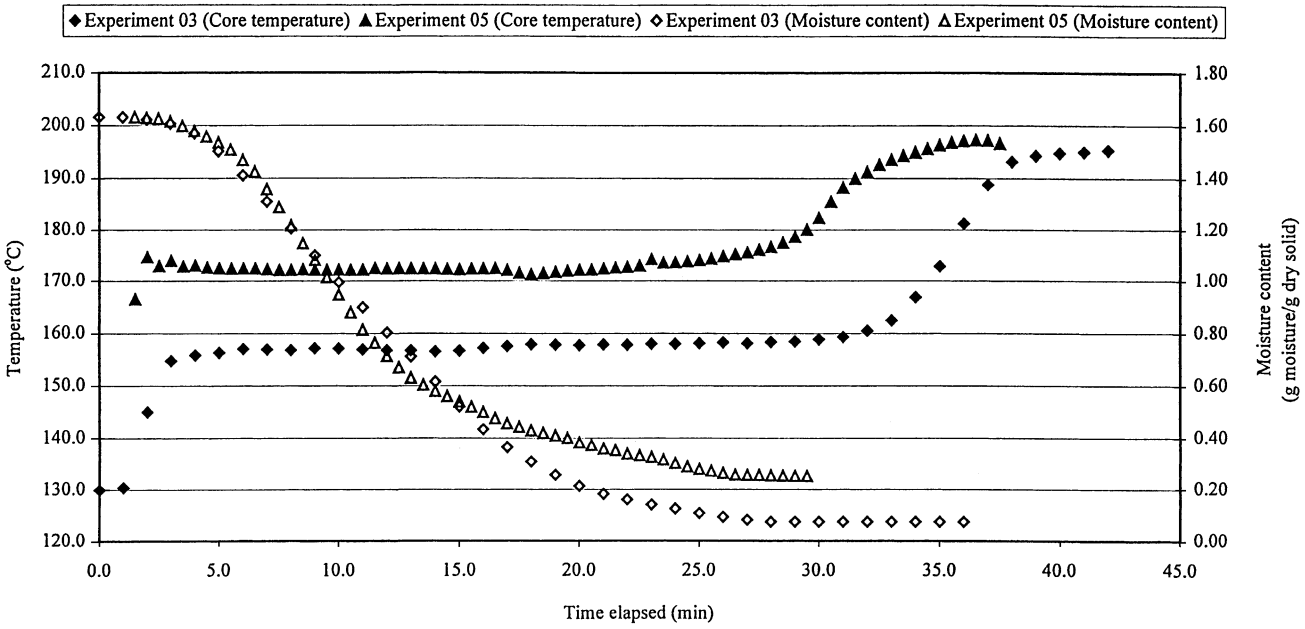

Fig. 3. Single coal particle drying at different pressures—Experiment 03: 12 mm, 1.5 m/s steam at 5.8 bar, 195 °C; Experiment 05: 12 mm, 1.4 m/s steam at 8.4 bar, 197 °C.

particles also vary during the course of drying [5]. The collapse of the pore structure when the moisture is expelled invariably results in the shrinking of the particles, which was visually observed at the end of each experiment. Previously published work [6] indicates that both the chemical and physical properties of coal change when subjected to a drying or dewatering process. Fig. 2 shows that the effects of the chemical and physical properties variations on the drying characteristics are consistent across independent experiments. The degree of reproducibility of the results indicates that the cracks observed on the coal particles were very likely to occur at the end of the experiments and that the drying process was not affected.

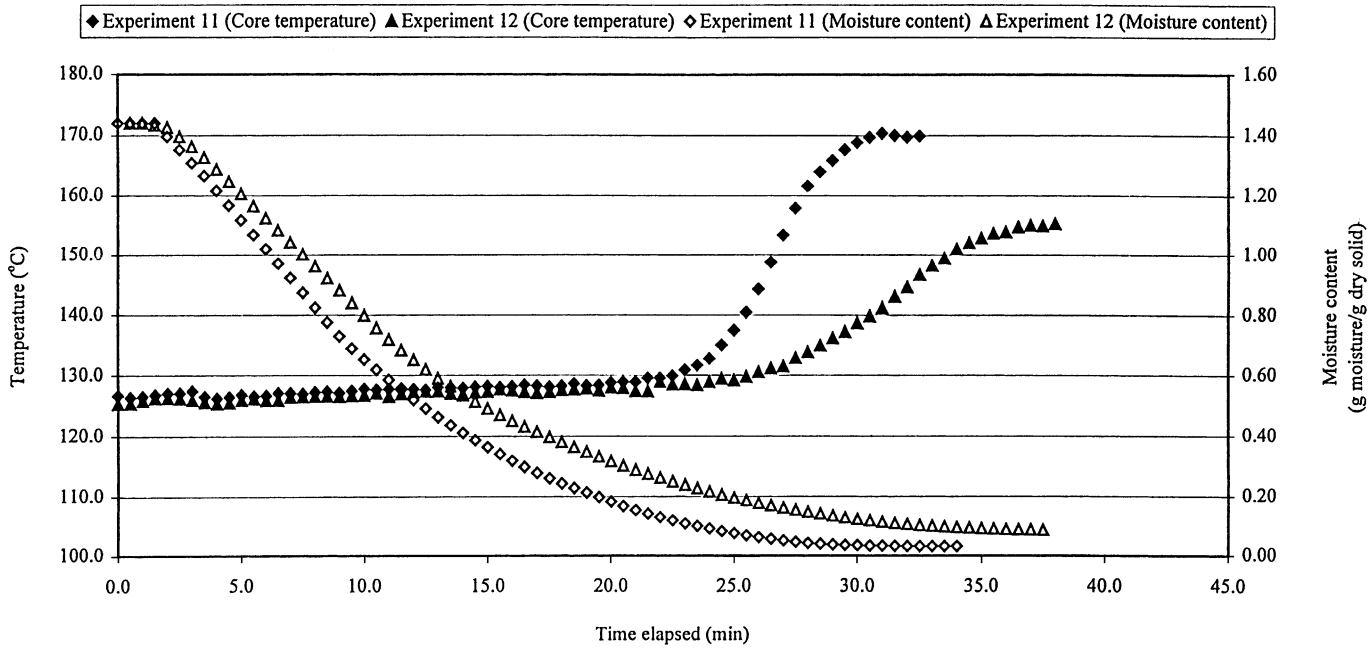

Fig. 4. Single coal particle drying at different temperatures—Experiment 11: 12 mm, 2.7 m/s steam at 2.5 bar, 170 °C; Experiment 12: 12 mm, 2.8 m/s steam at 2.5 bar, 155 °C.

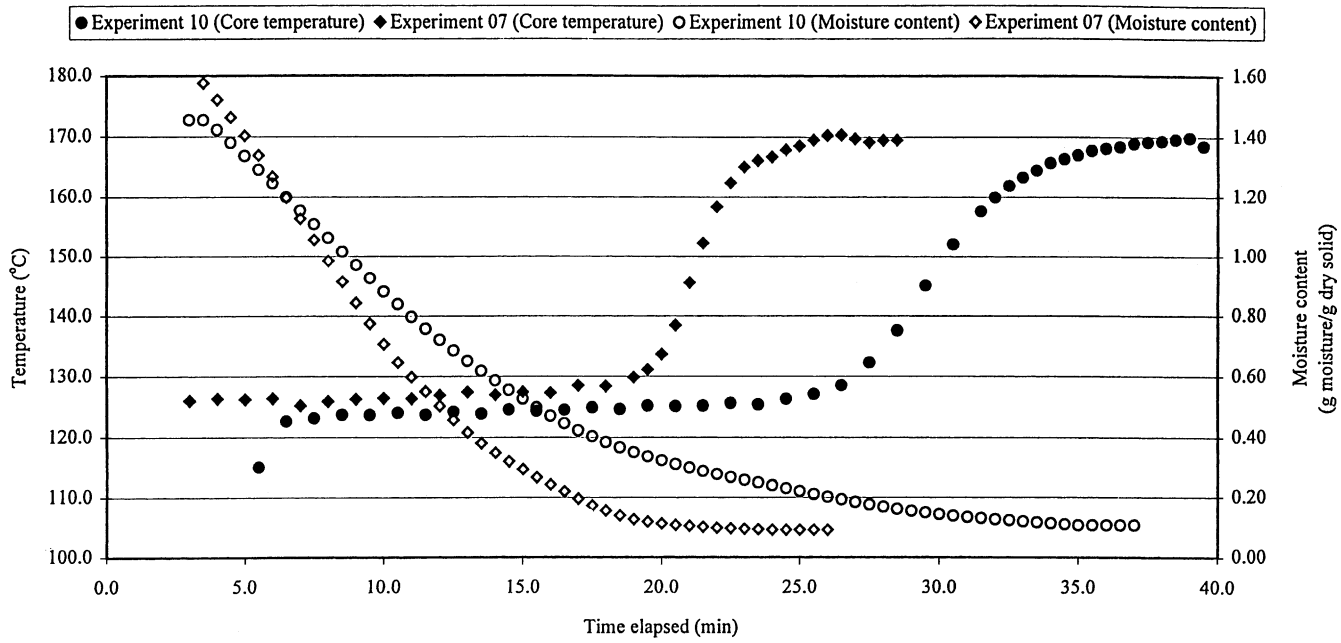

Fig. 5. Effect of particle sizes on single coal particle drying—Experiment 07: 10 mm, 2.7 m/s steam at 2.4 bar, 170 °C; Experiment 10: 12 mm, 2.7 m/s steam at 2.3 bar, 170 °C.

3.2. Pressure

The effect of pressure on the drying kinetics can be seen in Fig. 3. As expected, the initial core temperature of both Experiments 03 and 05 matched the saturated steam temperature at the prevailing pressure and the final core temperature for both cases approached the bulk superheated steam temperature.

The end point of drying, as indicated by the rise of core temperature, appears to occur earlier when drying is carried out in a higher pressure environment. There appears to be no influence of pressure on the drying rate but the

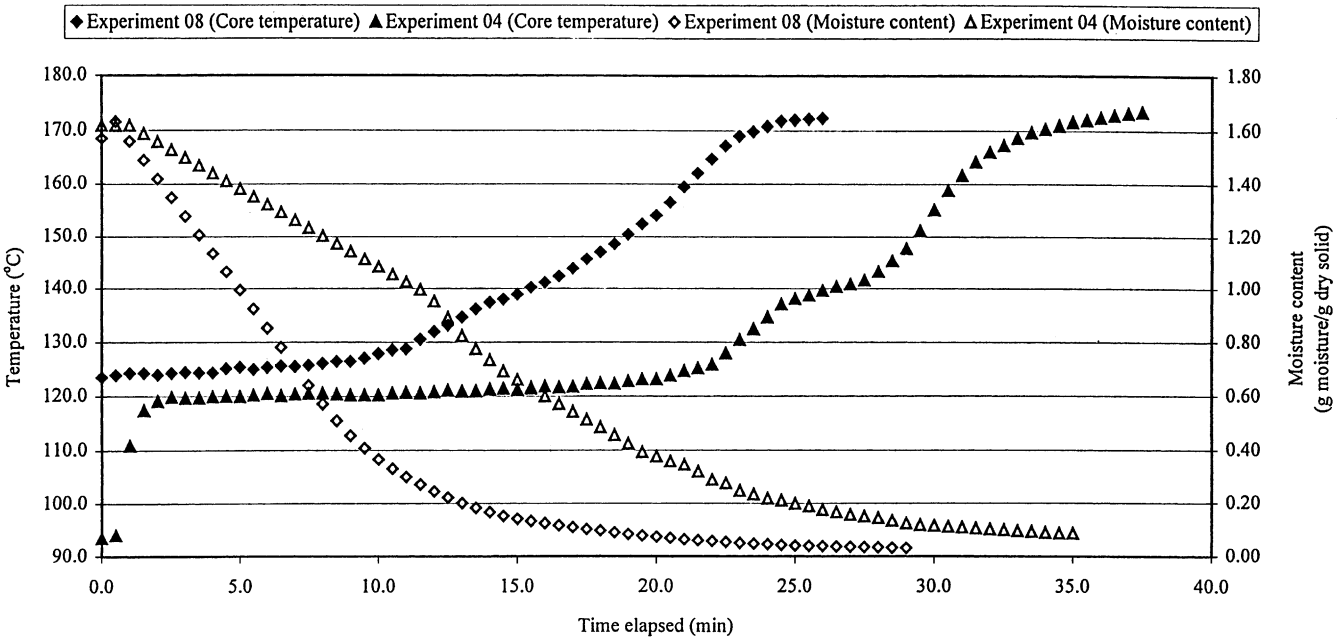

Fig. 6. Effect of steam velocity on single coal particle drying—Experiment 04: 12 mm, 2.7 m/s steam at 2.0 bar, 173 °C; Experiment 08: 12 mm, 3.5 m/s steam at 2.3 bar, 171 °C.

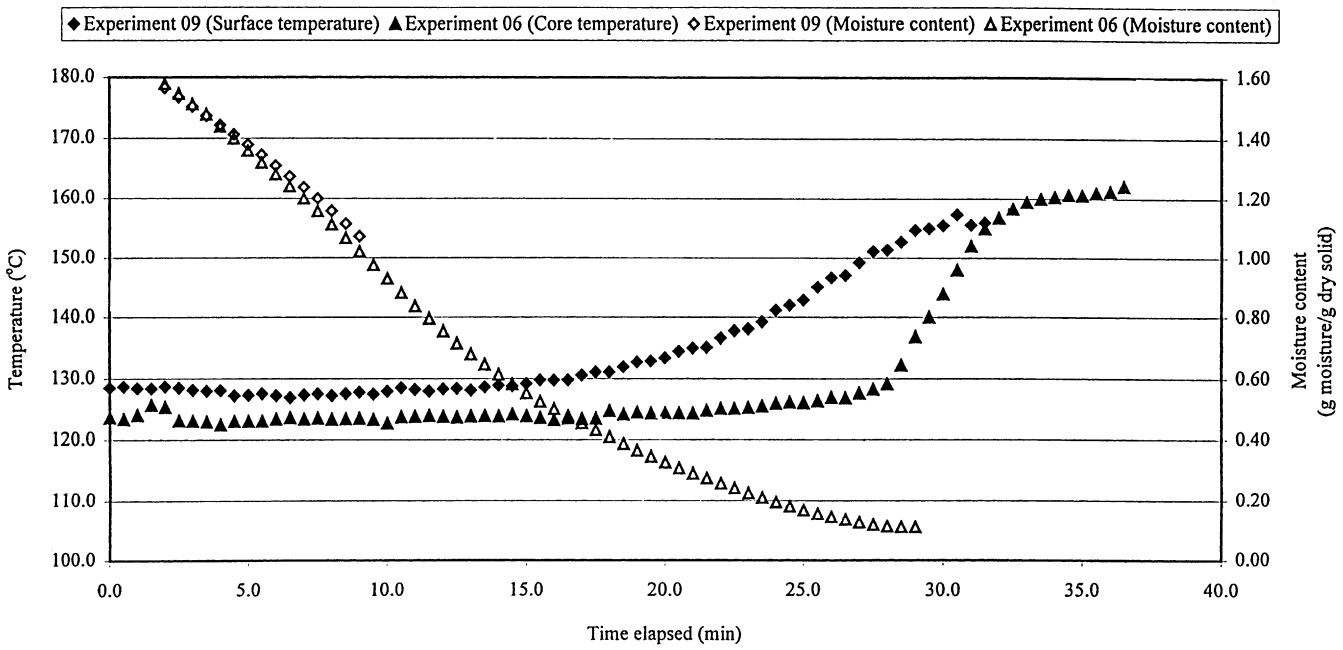

Fig. 7. Core and surface temperatures during single coal particle drying—Experiment 06: 12 mm, 2.7 m/s steam at 2.3 bar, 161 °C; Experiment 09: 12 mm, 2.8 m/s steam at 2.5 bar, 156 °C.

final moisture content is higher for the higher pressure operation. This shows that the equilibrium moisture content is higher in a higher pressure steam and the earlier completion of drying is due to the earlier establishment of equilibrium.

Forced convective heat transfer can be assumed to take place between the bulk steam and the particle surfaces in both cases. Using the correlation (Eq. (1)) proposed by Hager et al. [7], the heat transfer coefficients are calculated to be 115 and 135 W/m^2 K for Experiments 03 and 05, respectively. The marginal difference in the external heat transfer coefficient between the two experiments is consistent with the observed similar rate of moisture loss from the particles in both the experiments.

$$\frac{hd_p}{k_g} = 2 + 0.61Re^{0.52}\,Pr^{0.33} \quad (1)$$

The lack of pressure effect on the drying rate shows that the increase in the surrounding steam pressure from 5.8 to 8.4 bar does not contribute to a higher mass transfer resistance within the porous particles.

3.3. Superheated steam temperature

The influence of the bulk superheated steam temperature on the drying kinetics can be deduced from the results shown in Fig. 4. The data show that the core temperature rises earlier when a higher temperature steam is used. The rate of moisture loss is also more rapid when the drying is carried out in hotter steam. This higher drying rate is attributed to the increased rate of heat transfer from the bulk superheated steam to the particle and therefore it is shown that the drying rate is limited by the heat transfer rate.

3.4. Particle size

The effect of particle size on the drying rate is illustrated in Fig. 5. The external convective heat transfer coefficients for Experiments 07 and 10 were calculated using Eq. (1) and were found to be 117 and 107 W/m^2 K, respectively. The initial drying rate can be deduced from Fig. 5 as 0.044 and 0.067 g moisture/s, for Experiments 07 and 10, respectively.

If the drying rate is limited by the external heat transfer, the drying rate is expected to be proportional to the product of external heat transfer coefficient (h) and the particle surface area (A). The values of hA for Experiments 07 and 10 can be calculated to be 6.14×10^{-5} and 9.67×10^{-5} W/K, respectively. The ratio of these two values approximately match the ratio of the initial drying rates between Experiments 07 and 10. This provides further evidence for the rate of drying being limited by the external heat transfer rate.

3.5. Superheated steam velocity

Fig. 6 shows that a higher steam velocity results in a higher drying rate. This finding is consistent with the case that the drying of single particle within the operating range considered in this work is heat transfer limited.

There are two heat transfer mechanisms which may occur in this process; convective heat transfer from the bulk superheated steam to the particle surface and the conductive heat transfer from the surface to the core of

the particle. The steam flow variation does not influence the thermal conductivity within the porous particle. The fact that the steam velocity around the particle influences the drying rate is an indication that the drying rate limiting mechanism is indeed the external convective heat transfer.

3.6. Core and surface temperatures of particle

The temperature profile within a porous particle which is subjected to steam drying has been an ongoing dispute among the researchers in this area. Almost all the drying models available rely on the assumption on how the internal temperature varies with time [3,7,8].

The model proposed by Hager et al. [7] assumes that the temperature gradient within the porous particle is negligible. The particle temperature, according to that model [7], remains at the saturation point until the moisture content falls to a critical value when dry spots start to occur and the particle temperature starts to rise. In short, the temperature of the surface of the particle is expected to rise at the same time as that of the core of the particle.

On the other hand, the models similar to those by Shibata et al. [9] and Khan et al. [10], which are based on the receding core assumption, specify that evaporation occurs only at a drying front. The front moves from the surface of the particle to the core as drying progresses. The drying front assumes a singular saturated condition. The wet zone, between the front and the centre of the particle, remains below the saturated temperature while the temperature of dry zone, between the front and the surface of the particle, rises towards the surrounding temperature.

The experimental results presented in Fig. 7 show that the temperature of the particle surface rises earlier than that of the core of the particle. The temperature obtained in Experiment 09 was measured with the thermocouple junction located just underneath the surface of the coal particle. This observation supports the receding core assumption.

4. Numerical modelling

The numerical model employed in this work is based on a simple receding core model. This assumes that the evaporation of moisture occurs only on a defined drying front which is parallel with the particle surface. The model also assumes that mass transfer resistance is negligible. The only mass balance consideration is the evaporation of liquid moisture at the drying front. Heat is transferred from the surrounding superheated steam to the particle surface by convection while the radiative heat transfer component is neglected.

During the initial preheating period, the entire wet particle temperature is below the saturated steam temperature at the prevailing surrounding pressure. The sole mode of heat transfer occurring is by conduction as described by the following equation:

$$\frac{\partial T}{\partial t} = \alpha\left(\frac{2}{r}\frac{\partial T}{\partial r} + \frac{\partial^2 T}{\partial r^2}\right), \quad \alpha = \frac{k}{\rho C_p} \tag{2}$$

where k is the thermal conductivity, ρ the density, C_p the specific heat capacity, T the temperature, t the time and r is the radial position.

The temperature of the entire wet particle rises towards a thermal equilibrium state and the temperature gradient results in the particle surface temperature rising faster than that of the centre of the particle. The temperature profile is assumed to be symmetrical about the centre of the particle and the temperature gradient at the particle surface is approximated to be linear. Hence, the boundary conditions are as follows:

$$\frac{\partial T}{\partial r} = 0, \quad \text{for } r = 0 \tag{3}$$

$$k\frac{\partial T}{\partial r}\bigg|_{R_p^-} = h(T_a - T), \quad \text{for } r = R_p \neq R_F \tag{4}$$

where h is the external heat transfer coefficient, R_p the particle radius or radial position of particle surface, R_F the radial position of drying front and T_a is the surrounding temperature.

Drying commences when the particle surface temperature reaches the saturated steam temperature. The physical model can be distinctively sectioned into two zones; the dry zone is bounded by the particle surface and the drying front, whereas the wet zone is located in between the drying front and the centre of the particle. The front recedes towards the centre of the particle as drying proceeds with time. During the drying period, the heat transferred to the drying front is assumed to be entirely consumed to evaporate the liquid moisture.

The temperature on the drying front is fixed at a singular saturated point until the moisture content, w, at the drying front drops to a critical value. For the purpose of this work, the critical value, w^*, represents the final residual moisture content which is experimentally determined. The moisture content parameter throughout this model is defined as the mass ratio of liquid moisture to dry solid.

The problem is set up with the entire spherical particle "sliced" into a finite number of concentric shells. When w^* is reached, the drying front recedes a shell step towards the centre of the solid particle. When the drying front has receded from the solid particle surface, heat is conducted radially inwards from the particle surface to the drying front, while the temperature of the dried zone outside the drying front continues to rise. It is assumed that the void created by the expulsion of liquid moisture is filled by vapour. In this model, collapsing of pores and particle shrinkage are neglected.

The temperature gradient approaching the front from the particle surface is approximated to be linear. Hence, the

evaporation of moisture at the drying front is mathematically represented by

$$\frac{\dot{m}_{\text{evap}}}{A_{\text{F}}} h_{\text{fg}} = h(T_{\text{a}} - T_{\text{sat}}), \quad \text{for } r = R_{\text{F}} = R_{\text{p}} \tag{5}$$

$$\frac{\dot{m}_{\text{evap}}}{A_{\text{F}}} h_{\text{fg}} = k \left(\left. \frac{\partial T}{\partial r} \right|_{R_{\text{F}}^{+}} \right), \quad \text{for } r = R_{\text{F}} \neq R_{\text{p}} \tag{6}$$

where $\dot{m}_{\text{evap}}$ is the evaporation rate, A_{F} the area of drying front and h_{fg} is the latent heat of evaporation.

The end point of the simulation occurs when the drying front coincides with the centre of the particle.

4.1. Transport properties

There are effectively three species of material, dry skeletal solid, liquid moisture and vapour, which coexist within the porous particles. The physical properties of the skeletal solid are assumed to be constant regardless of temperature or pressure. The liquid moisture within the wet core is assumed to be at saturated condition. All the transport properties of the skeletal solid, liquid moisture and steam are obtained from [11,12].

In order to correctly represent the physical characteristics of the system, the effective transport properties are determined. The approach adopted by the authors of this paper is based on quantitative presence of each component, which is a simplified form compared to the relationships presented by Shibata et al. [9].

The density parameter is a form of capacitance, therefore the effective density is the summation of all contributing components. In the wet zone, it is assumed that all the pores are filled with liquid moisture. Therefore, the effective density of the wet zone is

$$\rho_{\text{eff,w}} = (1 - \varepsilon_{\text{l}})(1 + w)\rho_{\text{s}} \tag{7}$$

Taking into account the residual liquid moisture and the vapour which occupies the void vacated by the evaporation of liquid moisture, the effective density of the dry zone can be described as

$$\rho_{\text{eff,d}} = (1 - \varepsilon_{\text{v}})(1 + w^{*})\rho_{\text{s}} + \varepsilon_{\text{v}}\rho_{\text{v}} \tag{8}$$

The subscripts 'v', 'l' and 's' represent the vapour, liquid and solid components, respectively. ε and ρ are the mass fraction and the density, respectively, of the component denoted by the subscript.

The treatment for specific heat capacity is similar with that of density. Hence, the specific heat capacity in the wet zone becomes

$$C_{p,\text{eff,w}} = \frac{\rho_{\text{s}}}{\rho_{\text{eff,w}}}(1 - \varepsilon_{\text{l}})(C_{p,\text{s}} + wC_{p,\text{l}}) \tag{9}$$

Similarly, the specific heat capacity in the dry zone is

$$C_{p,\text{eff,d}} = \frac{\rho_{\text{s}}}{\rho_{\text{eff,d}}}(1 - \varepsilon_{\text{v}})(C_{p,\text{s}} + w^{*}C_{p,\text{l}}) + \frac{\rho_{\text{v}}}{\rho_{\text{eff,d}}}\varepsilon_{\text{v}}C_{p,\text{v}} \tag{10}$$

The effective thermal conductivity of the wet zone can be represented as

$$k_{\text{eff,w}} = k_{\text{s}}(1 - \varepsilon_{\text{l}}) + k_{\text{l}}\varepsilon_{\text{l}} \tag{11}$$

The effective thermal conductivity of the dry zone can be written as

$$k_{\text{eff,d}} = k_{\text{s}} + (k_{\text{l}} - k_{\text{s}})\varepsilon_{\text{l}}^{*} + (k_{\text{v}} - k_{\text{s}})\varepsilon_{\text{v}} \tag{12}$$

where

$$\varepsilon_{\text{l}}^{*} = \frac{1 - \varepsilon_{\text{v}}}{(\rho_{\text{l}}/w^{*}\rho_{\text{s}}) + 1} \tag{13}$$

4.2. Numerical approximation

The numerical model is solved by finite difference method. There are several numerical methods available to solve a moving boundary problem such as this. The general distinctions between these methods involve the manner in which the moving boundary is handled and the way the shell steps are defined. There are also those which are further simplified by applying assumptions to constrain a parameter [10] in order to stabilise the solution.

In order to simplify the computation, this model is solved by means of a one-dimensional constant and equally-spaced shell step approach. With the exception of the solution at the spatial boundary nodes, the partial differential equations are expanded using the Crank–Nicholson method. The

Table 2
Input parameters for single particle drying simulation[a]

Superheated steam conditions	
P (kPa)	290
T_{a} (°C)	160.4
v (m/s)	2.7
ρ_{a} (kg/m^3)	1.46
Solid particle dry properties	
d_{p} (m)	0.0099
ρ_{s} (kg/m^3)	1550
ε_{v}	0.41
k_{s} (W/m K)	1.3
$C_{p,\text{s}}$ (J/kg K)	880
w^{*} (kg water/kg dry solid)	0.0109
Initial conditions	
w_0 (kg water/kg dry solid)	0.223
T_0 (°C)	80
ε_{l}	0.41
Saturated moisture conditions	
k_{l} (W/m K)	0.688
$C_{p,\text{l}}$ (J/kg K)	4275
ρ_{l} (kg/m^3)	933
ρ_{v} (kg/m^3)	1.60
Simulation configurations	
Time interval (s)	0.1
Number of shell steps	50

[a] Reference: Experiment 13; Figs. 8 and 9.

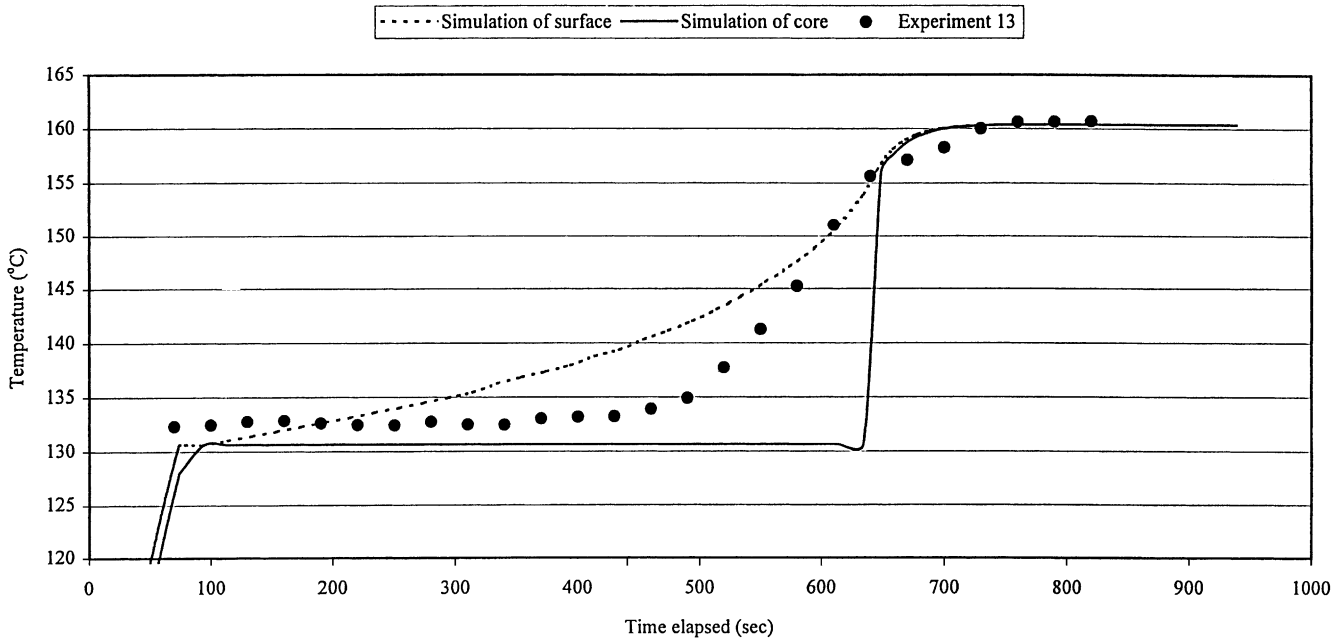

Fig. 8. Temperature simulation of ceramic particle drying—Experiment 13: 10 mm diameter, 2.7 m/s steam at 2.9 bar, 161 °C.

Crank–Nicholson method is based on the central difference approximation. It is therefore not applicable to the nodes which represent the particle surface. Hence, the expansion has to be modified to that of first order backward approximation. This problem does not arise when solving for the node at the particle centre because of the assumption of a symmetry.

4.3. Validation

This model has been tested against the drying results of ceramic particle drying. The input parameters for each simulation are tabulated in Table 2. Ceramic drying was considered because ceramic is physically more stable when subjected to superheated steam drying. The internal pore structure of

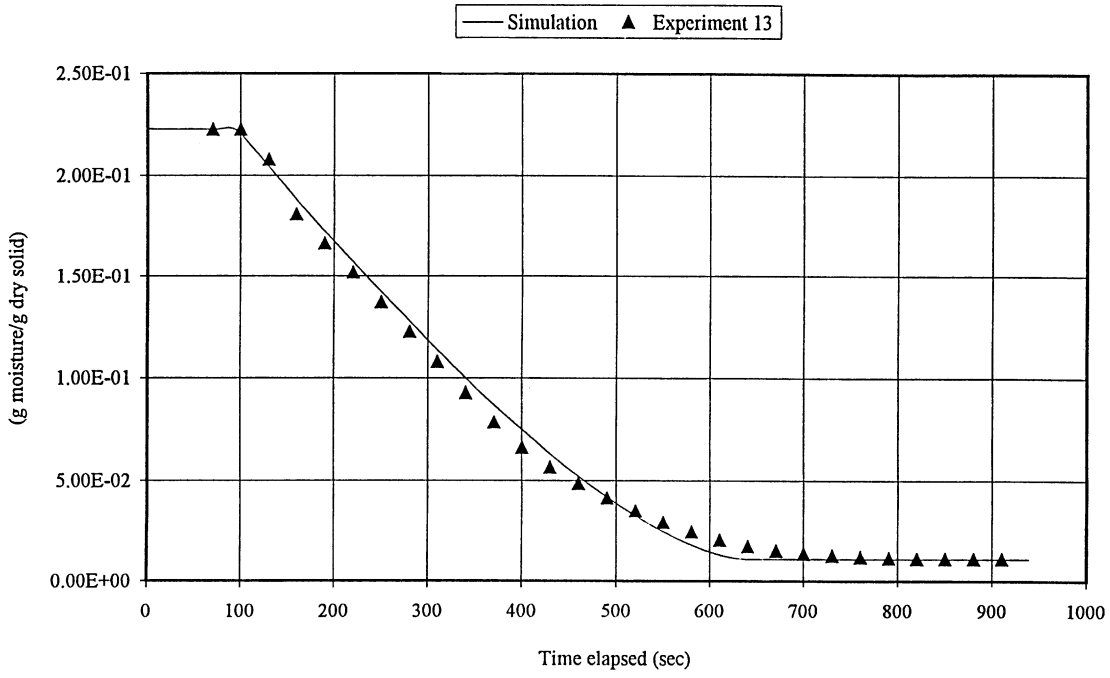

Fig. 9. Moisture content simulation of ceramic particle drying—Experiment 13: 10 mm diameter, 2.7 m/s steam at 2.9 bar, 161 °C.

the ceramic particle does not change during the course of drying, whereas the porosity of the coal particles has been known to vary. The degree of variation in coal particles is highly dependent on the conditions the samples are exposed to [7] and the quantifying of the change cannot be reliably done.

The comparison between the experimental results of Experiment 13 and the corresponding simulation is illustrated in Figs. 8 and 9. The experimentally measured core temperature also rises earlier than that the predicted value, although the time taken to arrive at the final temperature for both experimental work and simulation are in good agreement. Fig. 9 shows that for the ceramic particle the drying rate, the total drying time and the particle moisture content are all well predicted by the model.

A possible explanation for the discrepancy between predicted and measured core temperatures is that the thermocouple might not be measuring the temperature of the true centre of the particle. The conduction along the thermocouple could have resulted in the measurement of an average temperature around the thermocouple junction. A simplified estimation has shown that the energy conducted along the thermocouple wires could account for as much as 5% of the total energy delivered to the core. It is not easy to translate this into a temperature at the thermocouple junction, but we believe that this figure lends support to our suggestion that discrepancy between predicted and measured core temperatures is caused by errors in the measurement.

The attempts to validate the model against experimental lignite drying results indicated that the rate of moisture loss was under-predicted by the model. This is thought to be due to cracking of the lignite particles which increases the area for heat transfer. This under-prediction will be the subject of a future investigation.

5. Conclusions

A reliable experimental method has been developed to investigate the drying kinetics of single particles in pressurised superheated steam.

The end point of drying, as indicated by the rise of core temperature, appears to occur earlier when drying is carried out in a higher pressure environment. The operating pressure appears to have no influence on the drying rate. The experimental results, however, show that the equilibrium moisture content is higher in a higher pressure steam and that this equilibrium is attained earlier when drying is carried at higher pressure.

A simple receding core model for the drying of single particles in pressurised superheated steam has been developed and tested against the experimental results of ceramic particles. The validation shows that this model has the capability to predict the drying rate, total drying time and moisture content within a porous particle. Discrepancies between measured and predicted temperature profiles within the particles are thought to be due to measurement errors.

The experimental results of single lignite particles show that the rate of drying is limited by the rate of external convective heat transfer. These results, coupled with the simulation results, indicate that the evaporation of moisture occurs on a drying front which recedes towards the centre of the particle.

Acknowledgements

The authors gratefully acknowledge the financial and other supports received for this research from the Cooperative Research Centre Clean Power from Lignite, which is established under the Australian Government's Cooperative Research Centres program.

References

[1] E. Hausbrand, Drying by Means of Air and Steam, 3rd Revised English Edition, Scott, Greenwood & Sons, London, 1924.
[2] J. Karrer, Drying with Superheated Steam, Schweizerische Bauzeitung, 1920, pp. 228–230 (in German).
[3] M. Hermansson, R. Wimmerstedt, Steam drying of ceramic spheres—experiments and simulations, in: A.S. Mujumdar (Ed.), Proceedings of the Eighth International Drying Symposium (Drying'92), Que., Canada, 2–5 August 1992, Elsevier, Amsterdam, 1992, pp. 1215–1224.
[4] D.J. Allardice, The water in brown coal, in: R.A. Durie (Ed.), The Science of Victorian Brown Coal—Structure, Properties and Consequences for Utilisation, Butterworths/Heinemann, Oxford, 1991 (Chapter 3).
[5] G.D. Bongers, Brown coal drying process and aspects of fundamental coal structure, Ph.D. Thesis, Monash University, Melbourne, Australia, 1996.
[6] L.M. Clemow, P.J. Redlich, W.R. Jackson, R. Sakurovs, D.J. Allardice, The structure of raw brown coal and changes during drying, in: Proceedings of the Eighth Australian Coal Science Conference, The University of New South Wales, Sydney, Australia, 7–9 December 1998, pp. 195–200.
[7] J. Hager, M. Hermansson, R. Wimmerstedt, Modelling steam drying of a single porous ceramic sphere: experiments and simulations, Chem. Eng. Sci. 52 (8) (1997) 1253–1264.
[8] C. Moyne, D. Stemmelen, A. Degiovanni, Asymmetric drying of porous materials at high temperature. Theoretical analysis and experiments, Int. Chem. Eng. 30 (4) (1990) 654–671.
[9] H. Shibata, J. Mada, H. Shinohara, Drying mechanism of sintered spheres of glass beads in superheated steam, Ind. Eng. Chem. Res. 27 (1988) 2353–2362.
[10] J.A. Khan, D.E. Beasley, B. Alatas, Evaporation from a packed bed of porous particles into superheated vapor, Int. J. Heat Mass Transfer 34 (1) (1991) 267–280.
[11] R.H. Perry, D.W. Green (Eds.), Perry's Chemical Engineers' Handbook, 7th Edition, McGraw-Hill, New York, 1998.
[12] R.A. Durie (Ed.), The Science of Victorian Brown Coal—Structure, Properties and Consequences for Utilisation, Butterworths/Heinemann, Oxford, 1991.